molecular pharmaceutics

articles

Computational Models for Drug Inhibition of the Human Apical Sodium-Dependent Bile Acid Transporter

Xiaowan Zheng,[†] Sean Ekins,[†,‡,§] Jean-Pierre Raufman,[||] and James E. Polli*[,†]

Department of Pharmaceutical Sciences, School of Pharmacy, University of Maryland, 20 Penn Street, Baltimore, Maryland 21201, Collaborations in Chemistry, 601 Runnymede Avenue, Jenkintown, Pennsylvania 19046, Department of Pharmacology, University of Medicine & Dentistry of New Jersey (UMDNJ)—Robert Wood Johnson Medical School, 675 Hoes Lane, Piscataway, New Jersey 08854, and Department of Medicine, Division of Gastroenterology and Hepatology, University of Maryland School of Medicine, 22 South Greene Street, Baltimore, Maryland 21201

Received June 30, 2009; Revised Manuscript Received August 11, 2009; Accepted August 12, 2009

Abstract: The human apical sodium-dependent bile acid transporter (ASBT; SLC10A2) is the primary mechanism for intestinal bile acid reabsorption. In the colon, secondary bile acids increase the risk of cancer. Therefore, drugs that inhibit ASBT have the potential to increase the risk of colon cancer. The objectives of this study were to identify FDA-approved drugs that inhibit ASBT and to derive computational models for ASBT inhibition. Inhibition was evaluated using ASBT-MDCK monolayers and taurocholate as the model substrate. Computational modeling employed a HipHop qualitative approach, a Hypogen quantitative approach, and a modified Laplacian Bayesian modeling method using 2D descriptors. Initially, 30 compounds were screened for ASBT inhibition. A qualitative pharmacophore was developed using the most potent 11 compounds and applied to search a drug database, yielding 58 hits. Additional compounds were tested, and their K_i values were measured. A 3D-QSAR and a Bayesian model were developed using 38 molecules. The quantitative pharmacophore consisted of one hydrogen bond acceptor, three hydrophobic features, and five excluded volumes. Each model was further validated with two external test sets of 30 and 19 molecules. Validation analysis showed both models exhibited good predictability in determining whether a drug is a potent or nonpotent ASBT inhibitor. The Bayesian model correctly ranked the most active compounds. In summary, using a combined *in vitro* and computational approach, we found that many FDA-approved drugs from diverse classes, such as the dihydropyridine calcium channel blockers and HMG CoA-reductase inhibitors, are ASBT inhibitors.

Keywords: Bile acids; ASBT; QSAR; Bayesian; SLC10A2; transporters; colon cancer

Introduction

Bile acids are primarily absorbed in the terminal ileum by active uptake via the apical sodium-dependent bile acid transporter (ASBT; SLC10A2). The bile acid pool in humans is about 3−5 g, which cycles six times daily and results in a turnover of 12−18 g of bile acid each day. Less than 0.5 g is lost in feces each day, reflecting the high capacity and efficiency of this transporter.[1−3] ASBT knockout mice exhibited malabsorption of bile acids.[4] In humans, inherited mutations in ASBT result in idiopathic intestinal bile acid

* Author to whom correspondence should be addressed: Department of Pharmaceutical Sciences, School of Pharmacy, University of Maryland, HSF2, Room 623, Baltimore, MD 21201. Tel: 410-706-8292. Fax: 410-706-5017. E-mail: jpolli@rx.umaryland.edu.

[†] School of Pharmacy, University of Maryland.

[‡] Collaborations in Chemistry.

[§] University of Medicine & Dentistry of New Jersey (UMDNJ)—Robert Wood Johnson Medical School.

[||] University of Maryland School of Medicine.

(1) Dawson, P. A.; Oelkers, P. Bile acid transporters. *Curr. Opin. Lipidol.* **1995**, *6*, 109–114.

(2) Dawson, P. A.; Lan, T.; Rao, A. Bile acid transporters. *J. Lipid Res.* **2009**. DOI: 10.1194/jlr.R900012-JLR200.

(3) Wong, M. H.; Rao, P. N.; Pettenati, M. J.; Dawson, P. A. Localization of the ileal sodium-bile acid cotransporter gene (SLC10A2) to human chromosome 13q33. *Genomics* **1996**, *33*, 538–540.

10.1021/mp900163d CCC: $40.75
Published on Web 08/12/2009

malabsorption syndrome (IBAM), suggesting that ASBT is the primary mechanism for intestinal bile acid reabsorption.[5−7]

Epidemiological and experimental studies implicate secondary bile acids (e.g., lithocholic and deoxycholic acids) as important factors in the development of colorectal cancer.[8−14] Correspondingly, reducing the proportion of fecal deoxycholic acid by feeding ursodeoxycholic acid decreases colon tumor formation.[15−17] The cellular mechanism for bile acids promoting colon cancer is still being investigated, although it is known that bile acids modulate cellular signaling cascades and interact with cellular receptors. For example, deoxycholic acids are effective modulators of key signaling pathways, including ERK,[18] AKT,[19] COX2,[20] PKC,[21] MAPK,[22] and EGFR.[23] ASBT inhibition or compromised ASBT function results in more bile acids passing into the colon, thereby increasing colonic epithelial exposure to secondary bile acids that may stimulate colon cancer cell proliferation and survival.[23] In fact, two studies observed an association between a polymorphism in the SLC10A2 gene and the risk of colorectal adenomatous polyps.[24,25]

Enhanced fecal bile acid levels due to ASBT inhibition could lead to a variety of other disorders. Bile acid malabsorption and subsequent interruption of bile acid enterohepatic circulation is associated with diarrhea, reduced plasma cholesterol levels, hypertriglyceridemia, and gallstone formation.[7,26−29] IBAM causes chronic diarrhea in early infancy and is often misdiagnosed as diarrhea-predominant irritable bowel syndrome.[7] ASBT inhibition by drugs has been suggested to cause bile acid-induced diarrhea.[30] Studies have found gallstone disease[29] is associated with diminished

(4) Shneider, B. L. Intestinal bile acid transport: biology, physiology, and pathophysiology. *J. Pediatr. Gastroenterol. Nutr.* **2001**, *32*, 407–417.

(5) Montagnani, M.; Love, M. W.; Rossel, P.; Dawson, P. A.; Qvist, P. Absence of dysfunctional ileal sodium-bile acid cotransporter gene mutations in patients with adult-onset idiopathic bile acid malabsorption. *Scand. J. Gastroenterol.* **2001**, *36*, 1077–1080.

(6) Wong, M. H.; Oelkers, P.; Dawson, P. A. Identification of a mutation in the ileal sodium-dependent bile acid transporter gene that abolishes transport activity. *J. Biol. Chem.* **1995**, *270*, 27228–27234.

(7) Oelkers, P.; Kirby, L. C.; Heubi, J. E.; Dawson, P. A. Primary bile acid malabsorption caused by mutations in the ileal sodium-dependent bile acid transporter gene (SLC10A2). *J. Clin. Invest* **1997**, *99*, 1880–1887.

(8) Hill, M. J.; Drasar, B. S.; Williams, R. E.; Meade, T. W.; Cox, A. G.; Simpson, J. E.; Morson, B. C. Faecal bile-acids and clostridia in patients with cancer of the large bowel. *Lancet* **1975**, *1*, 535–539.

(9) Hill, M. J. Bile acids and colorectal cancer: hypothesis. *Eur. J. Cancer Prev.* **1991**, *1 Suppl 2*, 69–74.

(10) Fernandez, F.; Caygill, C. P.; Kirkham, J. S.; Northfield, T. C.; Savalgi, R.; Hill, M. J. Faecal bile acids and bowel cancer risk in gastric-surgery patients. *Eur. J. Cancer Prev.* **1991**, *1* (Suppl. 2), 79–82.

(11) Reddy, B. S.; Wynder, E. L. Metabolic epidemiology of colon cancer. Fecal bile acids and neutral sterols in colon cancer patients and patients with adenomatous polyps. *Cancer* **1977**, *39*, 2533–2539.

(12) Reddy, B. S.; Narasawa, T.; Weisburger, J. H.; Wynder, E. L. Promoting effect of sodium deoxycholate on colon adenocarcinomas in germfree rats. *J. Natl. Cancer Inst.* **1976**, *56*, 441–442.

(13) Narisawa, T.; Magadia, N. E.; Weisburger, J. H.; Wynder, E. L. Promoting effect of bile acids on colon carcinogenesis after intrarectal instillation of N-methyl-N′-nitro-N-nitrosoguanidine in rats. *J. Natl. Cancer Inst.* **1974**, *53*, 1093–1097.

(14) Nagengast, F. M.; Grubben, M. J.; van Munster, I. P. Role of bile acids in colorectal carcinogenesis. *Eur. J. Cancer* **1995**, *31A*, 1067–1070.

(15) Earnest, D. L.; Holubec, H.; Wali, R. K.; Jolley, C. S.; Bissonette, M.; Bhattacharyya, A. K.; Roy, H.; Khare, S.; Brasitus, T. A. Chemoprevention of azoxymethane-induced colonic carcinogenesis by supplemental dietary ursodeoxycholic acid. *Cancer Res.* **1994**, *54*, 5071–5074.

(16) Narisawa, T.; Fukaura, Y.; Terada, K.; Sekiguchi, H. Prevention of N-methylnitrosourea-induced colon tumorigenesis by ursodeoxycholic acid in F344 rats. *Jpn. J. Cancer Res.* **1998**, *89*, 1009–1013.

(17) Pardi, D. S.; Loftus, E. V., Jr.; Kremers, W. K.; Keach, J.; Lindor, K. D. Ursodeoxycholic acid as a chemopreventive agent in patients with ulcerative colitis and primary sclerosing cholangitis. *Gastroenterology* **2003**, *124*, 889–893.

(18) Debruyne, P. R.; Bruyneel, E. A.; Li, X.; Zimber, A.; Gespach, C.; Mareel, M. M. The role of bile acids in carcinogenesis. *Mutat. Res.* **2001**, *480−481*, 359–369.

(19) Dent, P.; Fang, Y.; Gupta, S.; Studer, E.; Mitchell, C.; Spiegel, S.; Hylemon, P. B. Conjugated bile acids promote ERK1/2 and AKT activation via a pertussis toxin-sensitive mechanism in murine and human hepatocytes. *Hepatology* **2005**, *42*, 1291–1299.

(20) Zhang, F.; Subbaramaiah, K.; Altorki, N.; Dannenberg, A. J. Dihydroxy bile acids activate the transcription of cyclooxygenase-2. *J. Biol. Chem.* **1998**, *273*, 2424–2428.

(21) Lau, B. W.; Colella, M.; Ruder, W. C.; Ranieri, M.; Curci, S.; Hofer, A. M. Deoxycholic acid activates protein kinase C and phospholipase C via increased Ca2+ entry at plasma membrane. *Gastroenterology* **2005**, *128*, 695–707.

(22) Qiao, D.; Stratagouleas, E. D.; Martinez, J. D. Activation and role of mitogen-activated protein kinases in deoxycholic acid-induced apoptosis. *Carcinogenesis* **2001**, *22*, 35–41.

(23) Raufman, J. P.; Shant, J.; Guo, C. Y.; Roy, S.; Cheng, K. Deoxycholyltaurine rescues human colon cancer cells from apoptosis by activating EGFR-dependent PI3K/Akt signaling. *J. Cell. Physiol.* **2008**, *215*, 538–549.

(24) Wang, W.; Xue, S.; Ingles, S. A.; Chen, Q.; Diep, A. T.; Frankl, H. D.; Stolz, A.; Haile, R. W. An association between genetic polymorphisms in the ileal sodium-dependent bile acid transporter gene and the risk of colorectal adenomas. *Cancer Epidemiol., Biomarkers Prev.* **2001**, *10*, 931–936.

(25) Grunhage, F.; Jungck, M.; Lamberti, C.; Keppeler, H.; Becker, U.; Schulte-Witte, H.; Plassmann, D.; Friedrichs, N.; Buettner, R.; Aretz, S.; Sauerbruch, T.; Lammert, F. Effects of common haplotypes of the ileal sodium dependent bile acid transporter gene on the development of sporadic and familial colorectal cancer: a case control study. *BMC Med. Genet.* **2008**, *9*, 70.

(26) Abraham, B.; Sellin, J. H. Drug-induced diarrhea. *Curr. Gastroenterol. Rep.* **2007**, *9*, 365–372.

(27) Duane, W. C. Abnormal bile acid absorption in familial hypertriglyceridemia. *J. Lipid Res.* **1995**, *36*, 96–107.

(28) Love, M. W.; Dawson, P. A. New insights into bile acid transport. *Curr. Opin. Lipidol.* **1998**, *9*, 225–229.

(29) Bergheim, I.; Harsch, S.; Mueller, O.; Schimmel, S.; Fritz, P.; Stange, E. F. Apical sodium bile acid transporter and ileal lipid binding protein in gallstone carriers. *J. Lipid Res.* **2006**, *47*, 42–50.

ASBT expression. The relationship between ASBT function and familial hypertriglyceridemia is inconclusive.[31,32] Therefore, drugs that inhibit ASBT have potential to promote bile acid-induced diarrhea, hypertriglyceridemia, gallstone disease, and colon cancer. Surprisingly, to our knowledge, no study has investigated the ability of FDA-approved drugs to inhibit ASBT.

The objectives of the present study were to identify drugs that inhibit ASBT and derive computational models for inhibition of ASBT. Several ASBT inhibitors have been developed as novel cholesterol-lowering compounds,[33−35] including 2164U90,[36,37] S-8921,[38,39] SC-435,[40,41] S-0960,[42] and R-146224.[43] Structure-binding activity relationships for the ASBT have been previously described.[44,45] In both studies, models were developed using data from bile acid analogues or novel inhibitors, rather than from FDA-approved drugs. We identified a large number of drugs from diverse classes as ASBT inhibitors and applied a three-dimensional (3D) common feature quantitative HipHop model, a three-dimensional quantitative structure−activity relationship (3D-QSAR) model, and a Bayesian model with 2D molecular descriptors to explore the basis for these interactions. These models were used to screen a database of drugs to prioritize compounds for testing and were further evaluated with test sets of compounds from our laboratory and the literature. The most potent inhibitors of ASBT in this study were found to be dihydropyridine calcium channel blockers (CCBs) and HMG-CoA reductase inhibitors (i.e., statins). Possible implications of such drugs to the development of potential side effects via ASBT inhibition are discussed.

Experimental Section

Materials. [^{3}H]-Taurocholic acid (10 μCi/mmol) was purchased from American Radiolabeled Chemicals, Inc. (St. Louis, MO). Sodium taurocholate was purchased from Sigma (St. Louis, MO). Fetal bovine serum (FBS), trypsin, and Dulbecco's modified Eagle's medium (DMEM) were purchased from Invitrogen Corporation (Carlsbad, CA). WST reagent was purchased from Roche Applied Science (Indianapolis, IN). All drugs and other chemicals were obtained

(30) Chassany, O.; Michaux, A.; Bergmann, J. F. Drug-induced diarrhoea. *Drug Saf.* **2000**, *22*, 53–72.
(31) Duane, W. C.; Hartich, L. A.; Bartman, A. E.; Ho, S. B. Diminished gene expression of ileal apical sodium bile acid transporter explains impaired absorption of bile acid in patients with hypertriglyceridemia. *J. Lipid Res.* **2000**, *41*, 1384–1389.
(32) Love, M. W.; Craddock, A. L.; Angelin, B.; Brunzell, J. D.; Duane, W. C.; Dawson, P. A. Analysis of the ileal bile acid transporter gene, SLC10A2, in subjects with familial hypertriglyceridemia. *Arterioscler. Thromb. Vasc. Biol.* **2001**, *21*, 2039–2045.
(33) Huang, H. C.; Tremont, S. J.; Lee, L. F.; Keller, B. T.; Carpenter, A. J.; Wang, C. C.; Banerjee, S. C.; Both, S. R.; Fletcher, T.; Garland, D. J.; Huang, W.; Jones, C.; Koeller, K. J.; Kolodziej, S. A.; Li, J.; Manning, R. E.; Mahoney, M. W.; Miller, R. E.; Mischke, D. A.; Rath, N. P.; Reinhard, E. J.; Tollefson, M. B.; Vernier, W. F.; Wagner, G. M.; Rapp, S. R.; Beaudry, J.; Glenn, K.; Regina, K.; Schuh, J. R.; Smith, M. E.; Trivedi, J. S.; Reitz, D. B. Discovery of potent, nonsystemic apical sodium-codependent bile acid transporter inhibitors (Part 2). *J. Med. Chem.* **2005**, *48*, 5853–5868.
(34) Tremont, S. J.; Lee, L. F.; Huang, H. C.; Keller, B. T.; Banerjee, S. C.; Both, S. R.; Carpenter, A. J.; Wang, C. C.; Garland, D. J.; Huang, W.; Jones, C.; Koeller, K. J.; Kolodziej, S. A.; Li, J.; Manning, R. E.; Mahoney, M. W.; Miller, R. E.; Mischke, D. A.; Rath, N. P.; Fletcher, T.; Reinhard, E. J.; Tollefson, M. B.; Vernier, W. F.; Wagner, G. M.; Rapp, S. R.; Beaudry, J.; Glenn, K.; Regina, K.; Schuh, J. R.; Smith, M. E.; Trivedi, J. S.; Reitz, D. B. Discovery of potent, nonsystemic apical sodium-codependent bile acid transporter inhibitors (Part 1). *J. Med. Chem.* **2005**, *48*, 5837–5852.
(35) Tollefson, M. B.; Vernier, W. F.; Huang, H. C.; Chen, F. P.; Reinhard, E. J.; Beaudry, J.; Keller, B. T.; Reitz, D. B. A novel class of apical sodium co-dependent bile acid transporter inhibitors: the 2,3-disubstituted-4-phenylquinolines. *Bioorg. Med. Chem. Lett.* **2000**, *10*, 277–279.
(36) Root, C.; Smith, C. D.; Winegar, D. A.; Brieaddy, L. E.; Lewis, M. C. Inhibition of ileal sodium-dependent bile acid transport by 2164U90. *J. Lipid Res.* **1995**, *36*, 1106–1115.
(37) Lewis, M. C.; Brieaddy, L. E.; Root, C. Effects of 2164U90 on ileal bile acid absorption and serum cholesterol in rats and mice. *J. Lipid Res.* **1995**, *36*, 1098–1105.
(38) Ichihashi, T. [Hypolipidemic drugs--ileal Na+/bile acid cotransporter inhibitors (S-8921 etc)]. *Nippon Rinsho* **2002**, *60*, 130–136.
(39) Ichihashi, T.; Izawa, M.; Miyata, K.; Mizui, T.; Hirano, K.; Takagishi, Y. Mechanism of hypocholesterolemic action of S-8921 in rats: S-8921 inhibits ileal bile acid absorption. *J. Pharmacol. Exp. Ther.* **1998**, *284*, 43–50.
(40) West, K. L.; Zern, T. L.; Butteiger, D. N.; Keller, B. T.; Fernandez, M. L. SC-435, an ileal apical sodium co-dependent bile acid transporter (ASBT) inhibitor lowers plasma cholesterol and reduces atherosclerosis in guinea pigs. *Atherosclerosis* **2003**, *171*, 201–210.
(41) West, K. L.; Ramjiganesh, T.; Roy, S.; Keller, B. T.; Fernandez, M. L. 1-[4-[4[(4R,5R)-3,3-Dibutyl-7-(dimethylamino)-2,3,4,5-tetrahydro-4-hydroxy-1,1-dioxido-1-benzothiepin-5-yl]phenoxy]butyl]-4-aza-1-azoniabicyclo[2.2.2]octane methanesulfonate (SC-435), an ileal apical sodium-codependent bile acid transporter inhibitor alters hepatic cholesterol metabolism and lowers plasma low-density lipoprotein-cholesterol concentrations in guinea pigs. *J. Pharmacol. Exp. Ther.* **2002**, *303*, 293–299.
(42) Schlattjan, J. H.; Fehsenfeld, H.; Greven, J. Effect of the dimeric bile acid analogue S 0960, a specific inhibitor of the apical sodium-dependent bile salt transporter in the ileum, on the renal handling of taurocholate. *Arzneim. Forsch.* **2003**, *53*, 837–843.
(43) Kitayama, K.; Nakai, D.; Kono, K.; van der Hoop, A. G.; Kurata, H.; de Wit, E. C.; Cohen, L. H.; Inaba, T.; Kohama, T. Novel non-systemic inhibitor of ileal apical Na+-dependent bile acid transporter reduces serum cholesterol levels in hamsters and monkeys. *Eur. J. Pharmacol.* **2006**, *539*, 89–98.
(44) Swaan, P. W.; Szoka, F. C., Jr.; Oie, S. Molecular modeling of the intestinal bile acid carrier: a comparative molecular field analysis study. *J. Comput.-Aided Mol. Des* **1997**, *11*, 581–588.
(45) Baringhaus, K. H.; Matter, H.; Stengelin, S.; Kramer, W. Substrate specificity of the ileal and the hepatic Na(+)/bile acid cotransporters of the rabbit. II. A reliable 3D QSAR pharmacophore model for the ileal Na(+)/bile acid cotransporter. *J. Lipid Res.* **1999**, *40*, 2158–2168.

from Sigma Chemical (St. Louis, MO), Alexis Biochemicals (San Diego, CA), AK Scientific (Mountain View, CA), LKT Laboratories (St. Paul, MN), Spectrum Chemicals & Laboratory Products (Gardena, CA), Spectrum Pharmacy Products (Tucson, AZ), or TCI America (Portland, OR).

Cell Culture. Stably transfected ASBT-MDCK cells were grown at 37 °C, 90% relative humidity, and 5% CO_2 atmosphere and fed every two days.[46] Media comprised DMEM supplemented with 10% FBS, 50 units/mL penicillin, and 50 μg/mL streptomycin. Geneticin was used at 1 mg/mL to maintain selection pressure. Cells were passaged every 4 days or after reaching 90% confluence.

Inhibition Study. After reaching 90% confluence, cells were seeded in 12 well cluster plates (3.8 cm^2) at a density of 1.5 million cells/well and cultured for four days. The culture medium was changed every 48 h. To enhance ASBT expression, cells were treated with 10 mM sodium butyrate for 12−17 h at 37 °C. Uptake studies were performed on the fifth day and were conducted both in presence of Hanks' balanced salt solution (HBSS) with 137 mM NaCl and modified HBSS sodium-free buffer where sodium chloride was replaced by tetraethylammonium chloride. Since ASBT is a sodium-dependent transporter, studies using sodium-free buffer enabled the measurement of passive permeability of taurocholate. Cells were washed thrice with HBSS or sodium-free buffer. Cells were exposed to donor solution containing 2.5 μM taurocholate (spiked with 0.5 μCi/mL [^{3}H]-taurocholate) in the presence or absence of drug (at eight different concentrations, for most drugs) at 37 °C and 50 rpm orbital shaking for 10 min. The donor solution was removed, and the cells were washed thrice with ice-cold sodium-free buffer. Subsequently, cells were lysed using 0.25 mL of 1 M NaOH for 2 h at room temperature and neutralized with 0.25 mL of 1 M HCl. Cell lysate was then counted for associated radioactivity using a liquid scintillation counter. J_{max} of taurocholate was measure on each inhibition study occasion. Unless otherwise noted, data are summarized as mean (±SEM) of three measurements.

Kinetic Analysis. Inhibition data were analyzed in terms of inhibition constant K_i and a modified Michaelis−Menten competitive inhibition model (eq 1) that takes into account aqueous boundary layer (ABL) resistance.[47]

$$J = \frac{P_{ABL}\left(\frac{J_{max}}{K_t\left(1 + \frac{I}{K_i}\right) + S} + P_p\right)}{P_{ABL} + \frac{J_{max}}{K_t\left(1 + \frac{I}{K_i}\right) + S} + P_p}(S) \qquad (1)$$

where J is taurocholate flux, J_{max} and K_t are the Michaelis−Menten constants for ASBT-mediated transport, S is taurocholate concentration, P_p is the passive taurocholate permeability, I is the inhibitor concentration, K_i is the inhibition constant, and P_{ABL} is the aqueous boundary layer permeability (i.e., 150 $\times$ 10^{-6} cm/s).[47] K_t was 5.03 μM, obtained from a pooled data analysis approach. J_{max} was estimated from taurocholate uptake studies at high taurocholate concentrations where transporter was saturated (i.e., 200 μM); J_{max} estimates were corrected for passive taurocholate flux using sodium-free flux data, where $J_{max} = J_{\text{with sodium (HBSS)}} - J_{\text{without sodium (sodium-free buffer)}}$. P_p was estimated from taurocholate uptake studies in absence of sodium. K_i was estimated by using nonlinear regression fitting performed by WinNonlin Professional (Pharsight Corporation; Mountain View, CA).

Dixon Plot Analysis. Inhibition studies of taurocholate were performed as described above. The donor solution contained 0.5 μCi/mL [^{3}H]-taurocholate, cold taurocholate (1, 2.5, and 5 μM), and inhibitor (5, 25, and 50 μM). Modified Michaelis−Menten competitive (eq 1) and noncompetitive (eq 2) inhibition models were fitted to the uptake data.

$$J = \frac{P_{ABL}\left(\frac{J_{max}}{(K_t + S)\left(1 + \frac{I}{K_i}\right)} + P_p\right)}{P_{ABL} + \frac{J_{max}}{(K_t + S)\left(1 + \frac{I}{K_i}\right)} + P_p}(S) \qquad (2)$$

K_i was estimated by this nonlinear regression. The Akaike Information Criterion (AIC) from eq 1 and eq 2 fits was used in selecting the better fitting model as either competitive or noncompetitive inhibition.

Qualitative Pharmacophore Development and Database Screening. Computational molecular modeling studies were carried out using Catalyst in Discovery Studio 2.1 (Accelrys; San Diego, CA). The qualitative pharmacophore was developed based on 11 compounds (Table 1) using the HipHop method.[48] A pharmacophore attempts to describe the arrangement of key features that are important for biological activity. This pharmacophore was then applied to screen the SCUT database (796 compounds including drugs in the SCUT 2008 database plus additional metabolites and drugs of abuse) using the FAST search method, as previously

(46) Balakrishnan, A.; Sussman, D. J.; Polli, J. E. Development of stably transfected monolayer overexpressing the human apical sodium-dependent bile acid transporter (hASBT). *Pharm. Res.* **2005**, *22*, 1269–1280.

(47) Balakrishnan, A.; Hussainzada, N.; Gonzalez, P.; Bermejo, M.; Swaan, P. W.; Polli, J. E. Bias in estimation of transporter kinetic parameters from overexpression systems: Interplay of transporter expression level and substrate affinity. *J. Pharmacol. Exp. Ther.* **2007**, *320*, 133–144.

(48) Clement, O. O.; Mehl, A. T. HipHop: Pharmacophore based on multiple common-feature alignments. In *Pharmacophore perception, development, and use in drug design*; Guner, O. F., Ed.; International University Line: La Jolla, 2000; pp 69−84.

Table 1. Initial Screening Study for ASBT

compound	% inhibition[a]	K_i (μM)
thioridazine[b]	97.1	37.3 ± 4.0
amlodipine[b]	95.5	42.1 ± 7.7
indomethacin[b]	93.2	62.3 ± 4.6
bumetanide[b]	78.1	225 ± 17
mesoridazine[b]	73.6	17.6 ± 2.3
dibucaine[b]	68.8	34.7 ± 4.9
bendroflumethiazide[b]	64.5	92.7 ± 12.7
quinine[b]	59.9	223 ± 25
althiazide[b]	57.9	377 ± 79
probenecid[b]	47.4	385 ± 81
trichlormethiazide[b]	44.7	377 ± 79
ketoprofen	44.0	178 ± 29
labetalol	38.6	851 ± 104
anastrozole	36.8	402 ± 43
atropine	36.5	170 ± 22
ranitidine	30.2	886 ± 158
chlorothiazide	25.3	2020 ± 330
hydrochlorothiazide	25.8	1220 ± 140
scopolamine	15.9	6450 ± 1120
chloroquine	14.0	6320 ± 150
abacavir	13.1	5020 ± 880
meropenem	10.2	5010 ± 2600

[a] Percent inhibition of taurocholate uptake in the presence of 1000 μM concentration of the compound, compared to taurocholate uptake in the absence of the compound. Additionally, eight compounds are not listed since they caused less than 10% inhibition. [b] Compounds used in training set for the qualitative model.

described.[49] It was found that adding the van der Waals surface of the most active compound, mesoridazine, as a shape restriction could limit the number of hits returned.

Quantitative Pharmacophore Development. A 3D-QSAR was developed using the HypoGen method. The training set included 38 compounds from the CCB, statin, diuretic, and other drug classes. ASBT K_i values were used as the biological activity. In the HypoGen approach, ten hypotheses were generated using hydrophobic, hydrogen bond acceptor, hydrogen bond donor, and the positive and negative ionizable features. The inactive compounds were also used to add excluded volumes to the model. After assessing all ten generated hypotheses, the hypothesis with lowest energy cost was selected for further analysis, as this model possessed features representative of all the hypotheses and had the lowest total cost.

The total energy cost of the generated pharmacophore was calculated from the deviation between the estimated activity and the observed activity, combined with the complexity of the hypothesis (i.e., the number of pharmacophore features). A null hypothesis, which presumes that there is no relationship between chemical features and biological activities are normally distributed about their mean, was also calculated. Therefore, the greater the difference between the energy cost of the generated and null hypotheses, the less likely the generated hypothesis reflects a chance correlation. Also, the quality of the structure−activity correlation between the predicted and observed activity values was estimated via correlation coefficient.

Machine Learning with 2D Descriptors. Laplacian-corrected Bayesian classifier models were generated using Discovery Studio 2.1 (Accelrys, San Diego, CA).[50−54] Molecular function class fingerprints of maximum diameter 6 (FCFP_6), AlogP, molecular weight, number of rotatable bonds, number of rings, number of aromatic rings, number of hydrogen bond acceptors, number of hydrogen bond donors, and molecular fractional polar surface area were calculated from input sdf files using the "calculate molecular properties" protocol. The "create Bayesian model" protocol was used for model generation. A custom protocol for validation, involving leave 20% out 100 times, was used.

Results

Initial Screen. Initially, a wide range of 30 drugs of various therapeutic classes were selected and screened for human ASBT inhibition. A screening drug concentration of 1000 μM was used to detect a range of potencies, including weak inhibitors. At 1000 μM concentration, 11 compounds inhibited taurocholate uptake by at least 45%. Table 1 lists the screening result (i.e., percent inhibition) of these 11 drugs, along with their subsequently determined K_i values, which were obtained from taurocholate inhibition profiles by using eight different inhibitor concentrations. Among the remaining compounds, 11 drugs showed weak taurocholate inhibition (i.e., 10−45% inhibition). K_i values of these 11 weak inhibitors were also measured and are listed in Table 1. Eight compounds (cromolyn, dexamethasone, gefitinib, ketorolac, meropenem, methylprednisolone, prednisolone, and zidovudine) did not inhibit taurocholate uptake (i.e., less than 10% inhibition).

Qualitative Pharmacophore. The 11 drugs that provided the greatest inhibition from the initial screen study (Table

(49) Ekins, S.; Johnston, J. S.; Bahadduri, P.; D'Souza, V. M.; Ray, A.; Chang, C.; Swaan, P. W. In vitro and pharmacophore-based discovery of novel hPEPT1 inhibitors. *Pharm. Res.* **2005**, *22*, 512–517.

(50) Hassan, M.; Brown, R. D.; Varma-O'brien, S.; Rogers, D. Cheminformatics analysis and learning in a data pipelining environment. *Mol. Diversity* **2006**, *10*, 283–299.

(51) Klon, A. E.; Lowrie, J. F.; Diller, D. J. Improved naive Bayesian modeling of numerical data for absorption, distribution, metabolism and excretion (ADME) property prediction. *J. Chem. Inf. Model.* **2006**, *46*, 1945–1956.

(52) Prathipati, P.; Ma, N. L.; Keller, T. H. Global Bayesian models for the prioritization of antitubercular agents. *J. Chem. Inf. Model.* **2008**, *48*, 2362–2370.

(53) Rogers, D.; Brown, R. D.; Hahn, M. Using extended-connectivity fingerprints with Laplacian-modified Bayesian analysis in high-throughput screening follow-up. *J. Biomol. Screening* **2005**, *10*, 682–686.

(54) Bender, A.; Scheiber, J.; Glick, M.; Davies, J. W.; Azzaoui, K.; Hamon, J.; Urban, L.; Whitebread, S.; Jenkins, J. L. Analysis of pharmacology data and the prediction of adverse drug reactions and off-target effects from chemical structure. *ChemMedChem* **2007**, *2*, 861–873.

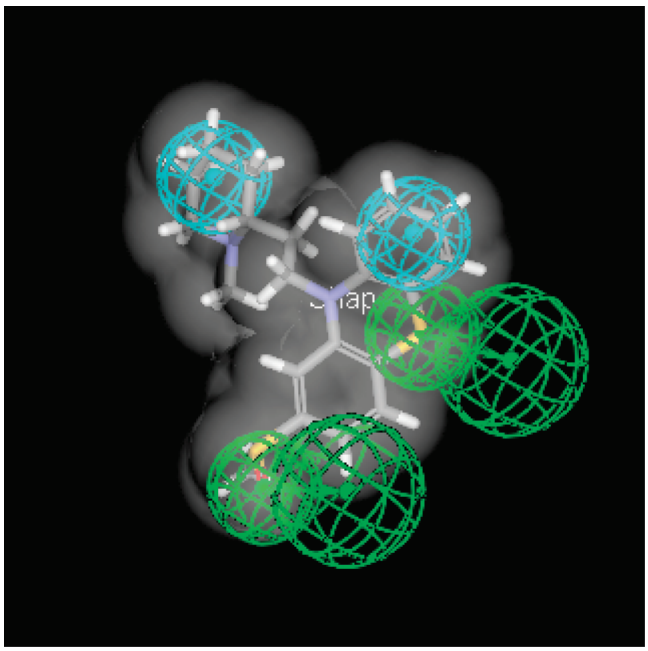

Figure 1. A HipHop pharmacophore of ASBT using the 11 most potent compounds from initial screening *in vitro*. The model consists of two hydrogen bond acceptors (green) and two hydrophobes (blue) features. Mesoridazine was used to create a shape restriction for the pharmacophore.

1) were used as training set (Table S1 in the Supporting Information) to develop a HipHop common features pharmacophore. Figure 1 illustrates the pharmacophore, which consisted of two hydrogen bond donors and two hydrophobic features. A shape restriction based upon the van der Waals shape of mesoridazine, which provided the most potent K_i in Table 1, was applied to the pharmacophore to limit the number of hits retrieved upon database searching.

The pharmacophore with a shape restriction was used to search the SCUT 2008 database. Fifty-eight compounds were retrieved as hits and listed in Table S2 in the Supporting Information, including their fit values. The quality of molecule mapping to the pharmacophore was reflected in the fit value, where the fit value depended on the proximity of the compound to the pharmacophore feature centroids and the weights assigned to each centroid. Higher fit value represents a better fit. Five drugs from the training set were retrieved as hits (i.e., amlodipine, bumetanide, indomethacin, mesoridazine, and thioridazine).

Secondary Screen. A secondary screen was conducted based on the 58 hits. Fifteen drugs were selected and assessed for ASBT inhibition. Drug selection was based on a wide range of fit values and compounds belonging to diverse therapeutic classes. As shown in Table 2, eight compounds were found to be potent inhibitors (K_i < 100 μM). Despite high fit values, enalapril did not inhibit ASBT and can be considered a false positive. Furosemide and pravastatin had low fit values and, as predicted, were indeed not potent inhibitors.

Table 2. Inhibition Results from Secondary Screening Study for ASBT

compound	fit value	K_i (μM)
thiothixene	3.758	808 ± 98
doxorubicin	3.142	101 ± 21
enalapril	3.049	10000[a]
aztreonam	2.973	1850 ± 360
nimodipine	2.829	5.75 ± 0.72
fluvastatin	2.565	11.5 ± 0.8
torasemide	2.277	292 ± 28
latanoprost	2.047	11.0 ± 2.0
lovastatin	1.733	21.6 ± 2.3
pentamidine	1.541	76.3 ± 19.2
simvastatin	1.503	10.4 ± 2.1
pravastatin	1.344	1360 ± 360
furosemide	0.959	5000[a]
pioglitazone	0.688	54.6 ± 10.3
tioconazole	0.5	33.1 ± 2.7

[a] K_i value was estimated from a single concentration and indicates drug was not a potent inhibitor.

Table 3. Inhibition Results from Calcium Channel Blockers, HMG-CoA Reductase Inhibitors and Diuretics

compound	K_i value (μM)	compound	K_i value (μM)
Calcium Channel Blockers			
nifedipine	3.87 ± 0.64	amlodipine[a]	42.1 ± 7.7
nisoldipine	4.77 ± 1.05	cilnidipine	45.2 ± 8.3
nimodipine[a]	5.75 ± 0.72	felodipine	49.7 ± 7.0
isradipine	19.4 ± 3.0	azelnidipine	85.6 ± 13.5
niguldipine	15.6 ± 2.6	manidipine	92.4 ± 21.1
nemadipine-A	23.1 ± 4.1	diltiazem	211 ± 21
nicardipine	32.4 ± 3.1	verapamil	266 ± 22
nitrendipine	34.1 ± 5.1		
HMG-CoA Reductase Inhibitors			
simvastatin[a]	10.4 ± 2.1	mevastatin	64.7 ± 9.2
fluvastatin[a]	11.5 ± 0.8	pravastatin[a]	1360 ± 360
lovastatin[a]	21.6 ± 2.3		
Diuretics			
bendroflumethiazide[a]	92.7 ± 12.7	indapamide	502 ± 78
spironolactone	110 ± 17	chlorthalidone	707 ± 58
bumetanide[a]	225 ± 17	cyclothiazide	1000[b]
trichlormethiazide[a]	377 ± 79	chlorothiazide[a]	1220 ± 140
althiazide[a]	391 ± 56	benzthiazide	1570 ± 440
torasemide[a]	292 ± 28	hydrochlorothiazide[a]	2020 ± 330
metolazone	456 ± 69	furosemide	5000[b]

[a] Compounds tested during initial or secondary screening. [b] K_i value was estimated from a single concentration and indicates drug was not a potent inhibitor.

Screen of CCBs, Statins and Diuretics. From initial and secondary screening studies, several CCBs (e.g., almodipine), statins (e.g., simvastatin), and diuretics (e.g., bendroflumethiazide) were found to be potent ASBT inhibitors. Therefore, further screening of drugs in these three classes was conducted. Table 3 shows the inhibition result in terms of K_i values. The results indicate that most of CCBs and statins were potent inhibitors, while almost all diuretics yielded K_i > 100 μM.

Fifteen CCBs were studied. Inhibition results show that the compounds in the dihydropyridine subclass (e.g., nife-

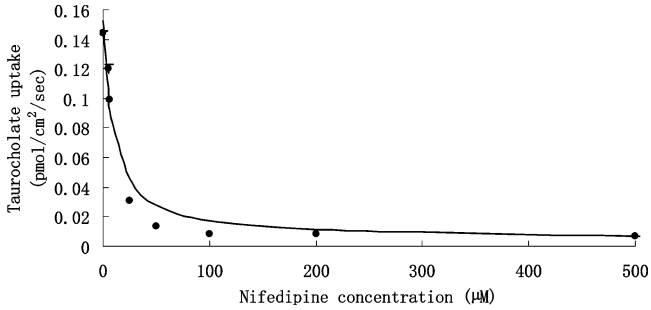

Figure 2. Concentration-dependent inhibition of taurocholate uptake into ASBT-MDCK monolayers by nifedipine. Cis-inhibition studies of taurocholate uptake were carried out at varying concentrations of nifedipine (0−500 μM). Closed circles indicate observed data points, while the solid line indicates model fit. Taurocholate uptake into ASBT-MDCK cells was reduced significantly by nifedipine, where $K_i = 3.87 \pm 0.64$ μM.

dipine, nimodipine, isradipine, nicardipine, nitrendipine, almodipine, and felodipine) were more potent inhibitors than most other types of CCBs (e.g., diltiazem and verapamil). Figure 2 illustrates the concentration-dependent inhibition of taurocholate uptake into ASBT-MDCK monolayers by nifedipine. Nifedipine was the most potent inhibitor, reducing taurocholate uptake over 10-fold and yielding a K_i of 3.87 μM.

Five statins were studied (Table 3), of which simvastatin, fluvastatin, lovastatin, and mevastatin were potent inhibitors, with K_i ranging from 10.4 to 64.7 μM. Meanwhile, pravastatin had a K_i of 1360 μM. Fourteen diuretic drugs were also studied. Except for bendroflumethiazide ($K_i = 92.7$ μM), all were nonpotent inhibitors (e.g., $K_i = 2020$ μM for hydrochlorothiazide).

Dixon plots were constructed for nifedipine (Figure 3A) and fluvastatin (Figure 3B), in order to characterize their mechanism of inhibition. For each drug, the lines converge above the *X*-axis, suggesting competitive inhibition of taurocholate uptake. Additionally the AIC from the nonlinear regression indicated the competitive inhibition model was better fitting than the noncompetitive inhibition model. In all these inhibition studies, it is assumed that inhibition is not via a non-ASBT mechanism.

Quantitative Pharmacophore. A 3D quantitative (HypoGen) pharmacophore was developed from 38 compounds. Table 4 lists the predicted as well as the observed K_i values of the training set. These compounds were selected as they reflect a range of K_i values over 1000-fold. The training set includes CCBs, statins, and diuretics (18 compounds), as well as drugs from diverse classes from the initial and secondary screens (20 compounds). The resulting quantitative pharmacophore with excluded volumes is illustrated in Figure 4. The pharmacophore was composed of one hydrogen bond acceptor, three hydrophobic features, and an additional five excluded volume features. Excluded volumes delineate the steric regions that were not occupied by active molecules, and this information is obtained from inactives in the data

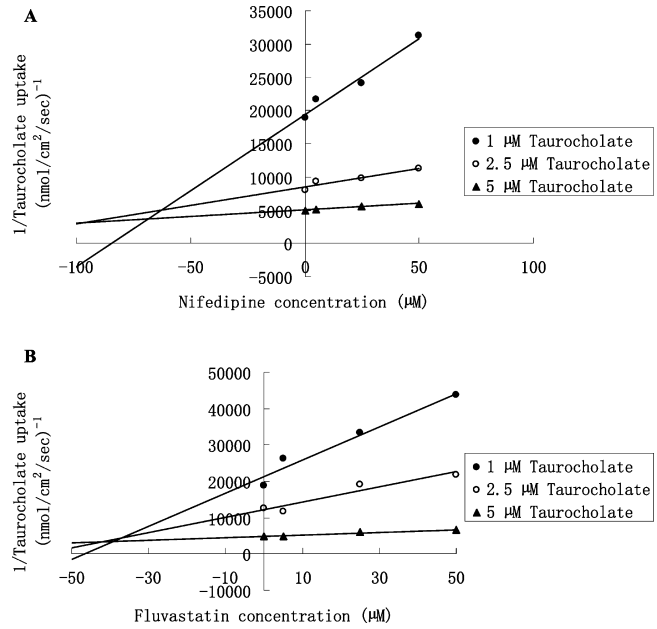

Figure 3. Dixon plot of nifedipine (A) and fluvastatin (B) inhibition of taurocholate uptake into ASBT-MDCK monolayer. Cis-inhibition studies of taurocholate uptake were carried out at varying concentrations of nifedipine (0, 5, 25, and 50 μM) and taurocholate (1, 2.5, and 5 μM). The three lines show the linear fits to taurocholate uptake data from experiments that employ taurocholate concentrations of 1 μM (filled circle), 2.5 μM (open square) and 5 μM (filled triangle).

set. The statistical significance of the generated hypothesis was assessed on the basis of its energy cost relative to the energy cost of the null hypothesis. Energy cost values for the generated hypothesis and null hypothesis were 145.1 and 189.7, respectively, indicating that the generated hypothesis was significant. The correlation coefficient reported from Catalyst was $r = 0.81$, reflecting an r^2 value for log(observed) versus log(predicted) K_i value of 0.66, which indicates that the model is acceptable.

This quantitative pharmacophore was successful in delineating potent inhibitors (i.e., $K_i < 100$ μM) from nonpotent inhibitors (i.e., $K_i > 100$ μM) for the compounds in the training set. In Table 5, results for each compound are characterized as true positives, false negatives, false positives, or true negatives. True positives are compounds that were both predicted and observed to be potent inhibitors. True negatives were both predicted and observed to be nonpotent inhibitors. False positives were predicted to be potent inhibitors but were not potent. False negatives were predicted to nonpotent inhibitors but were potent. The vast majority of training set compounds were correctly predicted, and there were no false positives, while only 10.5% of predictions were false negatives. Therefore, the quantitative pharmacophore exhibited good predictive power for the training set. A more important form of validation is using an external test set described later.

Bayesian Model. The same training set of 38 compounds used to generate the quantitative model was also applied to

Table 4. Training Set of 38 Compounds for the Quantitative Pharmacophore and Bayesian Model

quantitative pharmacophore					Bayesian model		
		K_i value (μM)					
compound	fit value	predicted[a]	obsd[b]	error[c]	compound	Bayesian score[d]	K_i value (μM), obsd
nifedipine	7.15	11	3.87 ± 0.64	2.8	nimodipine	21.5	5.75 ± 0.72
nimodipine	6.99	15	5.75 ± 0.72	2.7	nicardipine	21.1	32.4 ± 3.1
latanoprost	6.98	16	11.0 ± 2.0	1.4	nitrendipine	20.1	34.1 ± 5.1
simvastatin	6.93	18	10.4 ± 2.1	1.7	isradipine	17.4	19.4 ± 3.0
nitrendipine	6.93	18	34.1 ± 5.1	1.9	amlodipine	17.2	42.1 ± 7.7
isradipine	6.92	18	19.4 ± 3.0	1.1	nifedipine	17.0	3.87 ± 0.64
fluvastatin	6.89	20	11.5 ± 0.8	1.7	felodipine	16.5	49.7 ± 7.0
nicardipine	6.88	20	32.4 ± 3.1	1.6	simvastatin	13.4	10.4 ± 2.1
lovastatin	6.81	23	21.6 ± 2.3	1.1	lovastatin	11.8	21.6 ± 2.3
felodipine	6.48	50	49.7 ± 7.0	1	fluvastatin	11.6	11.5 ± 0.8
indomethacin	6.39	62	62.3 ± 4.6	1	tioconazole	11.4	33.1 ± 2.7
tioconazole	6.38	63	33.1 ± 2.7	1.9	pentamidine	10.8	76.3 ± 19.2
propafenone	6.33	71	62.0 ± 6.7	1.1	indomethacin	10.6	62.3 ± 4.6
amlodipine	6.12	110	42.1 ± 7.7	2.7	dibucaine	10.1	34.7 ± 5.0
pentamidine	5.83	220	76.3 ± 19.2	2.9	latanoprost	9.85	11.0 ± 2.0
quinine	5.83	220	223 ± 25	1	propafenone	9.03	62.0 ± 6.7
chloroquine	5.78	250	6320 ± 150	25	bendroflumethiazide	0.673	92.7 ± 12.7
dibucaine	5.77	260	34.7 ± 5.0	7.4	pravastatin	–1.89	1360 ± 360
bumetanide	5.73	280	225 ± 17	1.2	ketoprofen	–7.82	178 ± 29
ketoprofen	5.72	280	178 ± 29	1.6	labetalol	–10.9	851 ± 104
pravastatin	5.72	280	1360 ± 360	4.8	probenecid	–11.7	385 ± 81
prednisone	5.72	290	1480 ± 390	5.2	atropine	–12.8	170 ± 22
anastrozole	5.71	290	402 ± 43	1.4	diltiazem	–13.8	211 ± 21
aztreonam	5.69	310	1850 ± 360	6	chloroquine	–14.7	6320 ± 150
bendroflumethiazide	5.67	320	92.7 ± 12.7	3.5	anastrozole	–15.0	402 ± 43
spironoactone	5.65	330	110 ± 17	3	ranitidine	–15.6	886 ± 158
ranitidine	5.65	340	886 ± 158	2.6	triclomethiazide	–15.6	377 ± 79
thiothixene	5.64	350	808 ± 98	2.3	scopolamine	–16.3	6450 ± 1120
probenecid	5.62	360	385 ± 81	1.1	spironolactone	–16.3	110 ± 17
meropenem	5.62	360	1800 ± 450	5	hydrochlorthiazide	–16.4	2020 ± 330
althiazide	5.55	420	391 ± 56	1.1	prednisone	–18.4	1480 ± 390
atropine	5.53	440	170 ± 22	2.6	meropenem	–18.9	1800 ± 450
labetalol	5.47	510	851 ± 104	1.7	althiazide	–19.3	391 ± 56
diltiazem	5.45	540	211 ± 21	2.5	quinine	–19.3	223 ± 25
triclomethiazide	5.45	540	377 ± 79	1.4	aztreonam	–19.6	1850 ± 360
scopolamine	5.42	580	6450 ± 1120	11	bumetanide	–19.9	225 ± 17
abacavir	4.47	5100	5020 ± 880	1	abacavir	–22.4	5020 ± 880
hydrochlorthiazide	3.78	25000	2020 ± 330	12	thiothixene	–22.6	808 ± 98

[a] Predicted K_i values were obtained from the quantitative pharmacophore. [b] Observed K_i values were obtained from experimental measurements. [c] The values in the error column represent the ratio of the predicted activity to the observed activity, or its negative inverse if this ratio is less than one. [d] For the Bayesian model, the prediction was based on the Bayesian score and best split value (−1.085). If the score is higher than −1.085, the compound is predicted to be a potent inhibitor; a score lower than −1.085 predicted the compound to be nonpotent.

develop a Bayesian model[50] with molecular function class fingerprints of maximum diameter 6 (FCFP_6) and eight interpretable descriptors. The model had a leave-one-out cross-validation receiver operator curve (ROC) statistic of 0.91 (Table S3 in the Supporting Information) and enrichments (Tables S4 and S5 in the Supporting Information) that suggested that ASBT inhibitors (K_i < 100 μM) were well separated from noninhibitors (Table S6 in the Supporting Information). After leaving 20% out 100 times, the ROC [mean (±SD)] was 0.78 (±0.15); concordance was 72.5% (±18.4); specificity was 81.0% (±22.5); and sensitivity was 58.1% (±31.1). The Bayesian method showed favorable internal cross-validation, however the statistics for cross-validation may be impacted by the small training set when 20% are left out. Use of the FCFP_6 descriptors allowed the identification of molecular features that favored inhibition (Table S7A in the Supporting Information), as well as features that did not promote inhibition (Table S7B in the Supporting Information).

Table 4 lists the observed K_i values, as well as the Bayesian score of the training set. The best split value was −1.085 (Table S3 in the Supporting Information) and demarcated potent inhibitors from nonpotent inhibitors (Table 4). The best split value was calculated by minimizing the number of compounds that were incorrectly predicted as

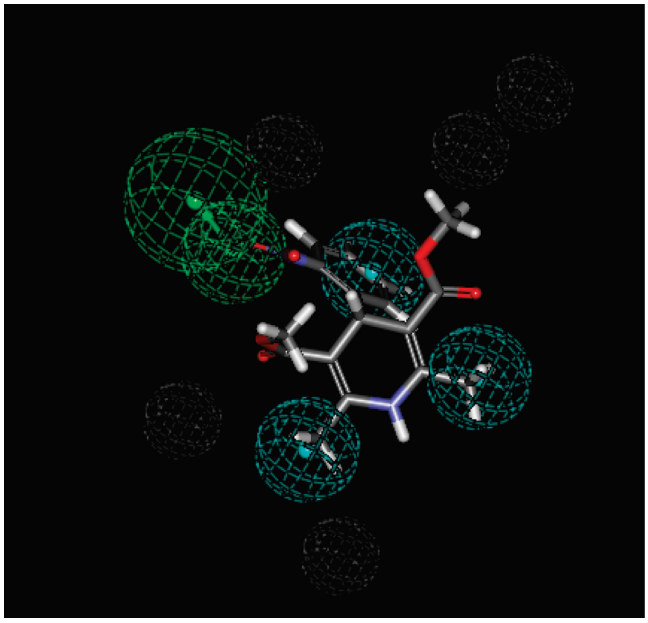

Figure 4. The quantitative Hypogen pharmacophore for hASBT derived from 38 molecules. Model features include one hydrogen bond acceptor (green), three hydrophobes (blue), and five excluded volumes (gray). The mapping of nifedipine to the pharmacophore is shown.

either potent or nonpotent inhibitors, using the cross-validated score for each sample. Based on the leave-one-out cross-validation method, the training set produced only 5.3% false negatives, and 5.3% false positives (Table 5 and Table S3 in the Supporting Information).

Test Set Evaluations. To validate the quantitative pharmacophore and the Bayesian model, 30 additional compounds were used as a first test set. These compounds exhibited over a 1000-fold range in K_i values and were not in the training set. This test set included CBBs, statins, diuretics, compounds from initial and secondary screening, and additional retrieved compounds from the SCUT 2008 database search. Table 6 lists the predicted and observed K_i values for the first test set using the quantitative model, and lists the score from the Bayesian model. Besides the first test set generated from experimental data in our laboratory, a second test set employed 19 chemically diverse bile acid analogues and ASBT inhibitors from the literature.[36,37,40,41,45] Table 7 lists the predicted K_i values, the reported IC_{50} values, and the Bayesian score for this literature test set.

Table 5 lists the numbers of compounds in each test set that were true positives, false negatives, false positives, or true negatives. For the quantitative model, the majority of the compounds in the first test set ($n = 30$) were correctly predicted with 10% of the predictions being false negative and 6.7% were false positive. For the Bayesian model, the majority were also correctly predicted while no prediction was a false negative and 16.7% were false positive.

Using the literature test set, which comprised bile acid analogues and potential ASBT inhibitors, both models showed poor predictability. Less than half of the compounds were correctly predicted to be either potent or nonpotent. In particular, both the quantitative pharmacophore and the Bayesian models provided a high false negative rate of 42.1% and 52.6%, respectively.

Discussion

Qualitative Pharmacophore. From the initial screen study, six potent ASBT inhibitors ($K_i < 100\ \mu M$) were identified: thioridazine, amlodipine, indomethacin, mesoridazine, dibucaine, and bendroflumethiazide. These compounds reflect a range of therapeutic drug classes, such as antipsychotics, CCBs, nonsteroidal anti-inflammatory drugs (NSAIDs), topical anesthetics, and diuretics. A qualitative pharmacophore was derived from initial screening data using the HipHop approach. The resulting pharmacophore with van der Waals surface shape restriction was used to search a database of FDA approved drugs. Eight potent inhibitors were further identified from this secondary screen study: nimodipine, fluvastatin, latanoprost, lovastatin, pentamidine, simvastatin, pioglitazone, and tioconazole. Each of these drugs is a member of the CCB, statin, antimicrobial, antihyperglycemic, or antifungal therapeutic drug class. Therefore, the qualitative HipHop pharmacophore served as a useful tool for drug screening, active compound identification, and further 3D-QSAR model development.

Quantitative Pharmacophore. The quantitative pharmacophore, derived from the HypoGen approach, was developed by using a training set of 38 compounds and included excluded volumes (Figure 4). Several recent reports have combined excluded volumes with a pharmacophore to improve models and predictions by identifying sterically inaccessible areas.[55−58] In the present report, automated refinement of the pharmacophore with excluded volume features provided a more selective model to reduce false positives for the first test set, yielding a better enrichment rate in virtual screening compared with the model without excluded volumes (Table S8 in the Supporting Information).

Bayesian Modeling. The Bayesian model correctly ranked the most active compounds. With zero false negatives for the first test set, it provided even better predictability for potent inhibitors than the quantitative pharmacophore provided. The Bayesian model with 2D fingerprints represents

(55) Greenidge, P. A.; Carlsson, B.; Bladh, L. G.; Gillner, M. Pharmacophores incorporating numerous excluded volumes defined by X-ray crystallographic structure in three-dimensional database searching: application to the thyroid hormone receptor. *J. Med. Chem.* **1998**, *41*, 2503–2512.

(56) Norinder, U. Refinement of Catalyst hypotheses using simplex optimisation. *J. Comput.-Aided Mol. Des* **2000**, *14*, 545–557.

(57) Palomer, A.; Cabre, F.; Pascual, J.; Campos, J.; Trujillo, M. A.; Entrena, A.; Gallo, M. A.; Garcia, L.; Mauleon, D.; Espinosa, A. Identification of novel cyclooxygenase-2 selective inhibitors using pharmacophore models. *J. Med. Chem.* **2002**, *45*, 1402–1411.

(58) Toba, S.; Srinivasan, J.; Maynard, A. J.; Sutter, J. Using pharmacophore models to gain insight into structural binding and virtual screening: an application study with CDK2 and human DHFR. *J. Chem. Inf. Model.* **2006**, *46*, 728–735.

Table 5. Validation Analysis for the Training and Test Sets[a]

	true positives[b]	false negatives[c]	false positives[d]	true negatives[e]
quantitative model training set ($n = 38$)	13 (34.2%)	4 (10.5%)	0 (0%)	21 (55.2%)
quantitative model test set ($n = 30$)	6 (20.0%)	3 (10.0%)	2 (6.7%)	19 (63.3%)
quantitative model literature test set ($n = 19$)	7 (36.8%)	8 (42.1%)	3 (15.8%)	1 (5.3%)
Bayesian model training set ($n = 38$)[f]	15 (39.5%)	2 (5.3%)	19 (50%)	2 (5.3%)
Bayesian model test set ($n = 30$)	9 (30.0%)	0 (0%)	5 (16.7%)	16 (53.3%)
Bayesian model literature set ($n = 19$)	5 (26.3%)	10 (52.6%)	1 (5.3%)	3 (15.7%)

[a] Values in table are numbers of compounds that were true positives, false negatives, false positives, or true negatives. Values in parentheses are simply the percent of compounds that were true positives, false positives, true negatives, or false negatives. [b] True positives were both predicted and observed to be potent inhibitors ($K_i < 100$ μM). [c] False negatives were predicted to nonpotent inhibitors but were potent. [d] False positives were predicted to be potent inhibitors but were not potent. [e] True negatives were both predicted and observed to be nonpotent inhibitors ($K_i > 100$ μM). [f] The calculation was based on the leave-one-out cross-validation approach.

Table 6. Test Set of 30 Compounds and Predictions with the Quantitative Pharmacophore and Bayesian Model

quantitative pharmacophore				Bayesian model		
		K_i value (μM)				
compound	fit value	predicted	obsd	compound	Bayesian score	K_i value (μM), obsd
cilnidipine	6.973	16.1	45.2 ± 8.3	cilnidipine	20.205	45.2 ± 8.3
azelnidipine	6.938	17.5	85.6 ± 13.5	manidipine	17.197	73.1 ± 13.3
nisoldipine	6.938	17.5	4.77 ± 1.05	niguldipine	16.554	15.6 ± 2.6
manidipine	6.868	20.5	73.1 ± 13.3	nisoldipine	16.3	4.77 ± 1.05
methylprednisolone	6.75	26.9	5000[a]	azelnidipine	11.989	85.6 ± 13.5
niguldipine	6.732	28.0	15.6 ± 2.6	nemadipine-A	11.071	23.1 ± 4.0
indapamide	6.661	33.0	501 ± 78	propafenone	9.034	62.0 ± 6.7
mevastatin	6.539	43.8	64.7 ± 9.2	mevastatin	8.729	64.7 ± 9.2
oseltamivir	6.172	102	5000[a]	pioglitazone	2.811	54.6 ± 10.3
dexamethasone	6.097	121	5000[a]	metolazone	1.631	456 ± 69
verapamil	6.035	140	266 ± 22	lisinopril	0.236	5000[a]
nemadipine-A	5.948	171	23.1 ± 4.0	enalapril	0.09	10000[a]
torasemide	5.746	272	292 ± 28	haloperidol	–0.156	5000[a]
famotidine	5.727	284	10000[a]	oseltamivir	–0.667	5000[a]
chlorthalidone	5.703	300	707 ± 58	darifenacin	–2.073	296 ± 34
darifenacin	5.699	303	296 ± 34	torasemide	–2.553	292 ± 28
pioglitazone	5.690	309	54.6 ± 10.3	cromolyn	–2.686	10000[a]
metolazone	5.680	316	456 ± 69	chlorthalidone	–2.995	707 ± 58
benzthiazide	5.662	329	1570 ± 440	gefitinib	–3.142	10000[a]
enalapril	5.660	331	10000[a]	indapamide	–3.263	501 ± 78
cromolyn	5.658	332	10000[a]	ketorolac	–4.13	10000[a]
propafenone	5.649	339	62.0 ± 6.7	famotidine	–4.213	10000[a]
gefitinib	5.605	376	10000[a]	benzthiazide	–5.317	1570 ± 440
cyclothiazide	5.583	396	1000[a]	zidovudine	–6.553	10000[a]
haloperidol	5.544	432	5000[a]	chlorothiazide	–6.949	1220 ± 140
furosemide	5.499	480	5000[a]	verapamil	–7.639	266 ± 22
lisinopril	5.413	585	5000[a]	dexamethasone	–9.998	5000[a]
ketorolac	5.361	659	10000[a]	methylprednisolone	–11.849	5000[a]
chlorothiazide	NM[b]		1220 ± 140	cyclothiazide	–13.709	1000[a]
zidovudine	NM		10000[a]	furosemide	–13.875	5000[a]

[a] K_i value was estimated from a single concentration and indicates drug was not a potent inhibitor. [b] NM denotes that the compound did not map to the pharmacophore.

a classification approach to building models that can be used for rapid screening of compound libraries.[52−54,59,60] Using molecular fingerprint descriptors identified regions in the training set molecules (e.g., the core dihydropyridine ring of some of the CCBs) that were likely important for ASBT inhibition (Table S7A in the Supporting Information), while substructures of other molecular features were associated with compounds that were not inhibitors (Table S7B in the Supporting Information).

(59) Metz, J. T.; Huth, J. R.; Hajduk, P. J. Enhancement of chemical rules for predicting compound reactivity towards protein thiol groups. *J. Comput.-Aided Mol. Des* **2007**, *21*, 139–144.

(60) Nidhi; Glick, M.; Davies, J. W.; Jenkins, J. L. Prediction of biological targets for compounds using multiple-category Bayesian models trained on chemogenomics databases. *J. Chem. Inf. Model.* **2006**, *46*, 1124–1133.

Table 7. Test Set of 19 Literature Compounds[36,37,40,41,45] and Predictions with the Quantitative Pharmacophore and Bayesian Model

quantitative pharmacophore			Bayesian model		
compound	K_i value (μM), predicted	IC_{50} value (μM)	compound	Bayesian score	IC_{50} value (μM)
S3740	18.7	8	S3740	4.023	8
S8211	20.5	4	S0381	1.089	700
S8005	23.4	3000	S0382	1.089	3
S0927	27	36	2164u90	0.662	7
S0925	30.6	16	Sc-435	–0.298	0.03
S9086	35	1500	S1690	–0.328	20
Sc-435	39.1	0.03	S1647	–2.158	4
S8214	39.9	4	S2305	–2.72	300
S2305	77.4	300	S0960	–2.89	30
S9202	79.1	90	S8005	–3.389	3000
S1647	134	4	S8211	–3.42	4
S0960	255	30	S9086	–3.457	1500
PB3	268	4	S9087	–3.457	0.3
S0381	275	700	PB3	–3.648	4
2164u90	326	7	S8214	–3.69	4
S1690	327	20	S9202	–4.38	90
S9087	NM[a]	0.3	S9203	–4.38	1
S9203	NM	1	S0925	–4.766	16
S0382	NM	3	S0927	–4.766	36

[a] NM denotes compound did not map to the pharmacophore.

Validation Results from Literature Test Set. While exhibiting good predictability for FDA-approved drugs, both models showed poor predictability for the test set that was composed of less-diverse literature ASBT inhibitors (Table 5 and Table 7). One possible explanation is that, for this data set, the literature IC_{50} values were generated using rabbit ASBT in CHO cells, while the computational models were generated using K_i values against human ASBT in MDCK cells. The sequence identity of the rabbit and human transporter is 85.67% and could manifest in different structure inhibitor relationships for each species. Some of the false negatives were bile acid analogues (i.e., compounds PB3, S1690 and S0960), while the computational models reported here were developed using drugs and not bile acids or bile acid analogues.

Comparison to Previous Pharmacophores. Two 3D-QSAR models have been developed for hASBT inhibitors. Swaan et al. studied the transport of a series of chemically homologous C-24 bile acid−peptide conjugates in Caco-2 monolayers and mapped the electrostatic and steric fields around bile acids through comparative molecular field analysis (CoMFA).[44,61] All conjugates carried a negative charge near the C-24 carbonyl. They concluded that the C-24 side chain could be at least 14 Å in length to allow for translocation, and that large hydrophobic moieties had increased binding to hASBT. As only chemically similar compounds were used for model generation, the model is silent on a number of regions due to lack of structural variability. The predictability of this model is likely limited, compared to the present 3D-QSAR model, which was able to predict the affinities of chemically diverse drugs. In addition, the CoMFA model is dependent upon molecule alignment, which is a known limitation of this method.

Kramer et al. developed a 3D-QSAR model using Catalyst of rabbit ASBT using 17 bile acid analogues and inhibitors.[45] The model was characterized by five chemical features: one hydrogen bond donor, one hydrogen bond acceptor, and three hydrophobic features. The model suggested that two hydroxyl groups of bile acid (C-3, C-7, or C-12) are optimal, the 3-hydroxyl group is not essential for binding, and vicinal hydroxyl groups on C-6 and C-7 drastically decrease affinity. However, the model did not explain or predict chemically diverse drugs and did not offer validation through further screening of compounds. Meanwhile, the current model employed a set of 38 diverse drugs to develop the model and 30 more drugs as a test set for validation. In addition, 19 literature-reported compounds, include the training set from Kramer's model, were used as a second test set to further validate the model, although the model performed poorly. Similarities between the current model and the model of Kramer et al. include a hydrogen bond acceptor and three hydrophobic features.

Drug Induced Potential Side Effects. ASBT inhibition can result in greater passage of bile acids into the colon, and thus is a possible mechanism for potential drug side effects such as diarrhea, gallstone disease, hypertriglyceridemia, decreased plasma cholesterol levels, and colon cancer. To our knowledge, no study has investigated the ability of FDA-approved drugs to inhibit ASBT *in vitro*. Several ASBT inhibitors that were developed as potential cholesterol-lowering drugs have not been approved to date.[33−43] In the

(61) Cramer, R. D., III.; Patterson, D. E.; Bunce, J. D. Recent advances in comparative molecular field analysis (CoMFA). *Prog. Clin. Biol. Res.* **1989**, *291*, 161–165.

present study, the most potent ASBT inhibitors were largely dihydropyridine, CCBs and statins. It is possible that chronic use of such drugs that are potent ASBT inhibitors has the potential to stimulate fecal bile acids and thus cause a variety of disorders or cause the development/progression of colon neoplasia. This is particularly true of drugs in extended-release formulations which may increase drug exposure in the terminal ileum where ASBT is expressed. For example nifedipine was found to be a potent ASBT inhibitor and is formulated for sustained release to treat hypertension.

Epidemiological studies have documented an association between colorectal cancer risk and elevations in fecal bile acid concentration, particularly lithocholic and deoxycholic acids.[8−11] Studies in rodents have shown that increasing fecal bile acid concentrations promotes the development of colon cancer.[12−14] Moreover, rats fed ursodeoxycholic acid show reduced proportions of fecal deoxycholic acid and decreased colon tumor formation.[15,16] In humans with inflammatory bowel disease, oral ursodeoxycholic acid modulates fecal bile acids and reduces the incidence of colorectal dysplasia and cancer.[17]

To date, epidemiological data regarding the association between the use of CCBs and cancer risk have been conflicting. Early epidemiologic studies have indicated that treatment with CCBs was associated with increased colon cancer incidence and mortality.[62−68] Subsequent studies have been negative or ambiguous; clinical trials have not demonstrated an increased cancer risk.[69−71] Studies have indicated that diuretic therapy was associated with an increased risk of colon cancer and colon cancer mortality. Experimental data indicate a possible preventive effect for statins in colorectal cancer.[72−77] However, the available epidemiological data are inconsistent.

Several pathophysiological mechanisms underlie drug-induced diarrhea. One possible mechanism is ASBT inhibition, resulting in excess bile acids reaching the colon thereby inducing secretory diarrhea.[30] Twelve to 25% of patients taking olsalazine report diarrhea, and olsalazine inhibits ASBT in rat.[78] Meanwhile, it is unclear that drugs identified to inhibit ASBT in the present study cause diarrhea. The frequency of diarrhea during HMG-CoA reductase inhibitor therapy (i.e., simvastatin, lovastatin, pravastatin) is less than 5%.[30] Observations of diarrhea induced by calcium antagonists (i.e., iradipine, nifedipine) also have been reported.[79,80] Other drugs with reported drug-induced diarrhea include ranitidine, diclofenac, aztreonam, and NSAIDS (i.e., indomethacin).[26,30] However, in reviewing these drug products' prescribing information, no relationship was clearly evident between the potency of a drug to inhibit ASBT and its association with diarrhea.

No strong evidence was easily evident here between drugs that are potent ASBT inhibitors and other possible side effects, such as plasma cholesterol, triglyceride levels, and gallstone disease. Limitations in relating the *in vitro* results here and potential side effects include unknown drug concentration in the terminal ileum and complex drug distribution effects. As ASBT is expressed in the terminal ileum, drug concentration in this gastrointestinal region

(62) Hardell, L.; Axelson, O.; Fredrikson, M. Antihypertensive drugs and risk of malignant diseases. *Lancet* **1996**, *348*, 542.
(63) Lindberg, G.; Lindblad, U.; Low-Larsen, B.; Merlo, J.; Melander, A.; Rastam, L. Use of calcium channel blockers as antihypertensives in relation to mortality and cancer incidence: a population-based observational study. *Pharmacoepidemiol. Drug Saf.* **2002**, *11*, 493–497.
(64) Pahor, M.; Furberg, C. D. Calcium antagonists and cancer: causation or association. *Cardiovasc. Drugs Ther.* **1998**, *12*, 511–513.
(65) Pahor, M.; Furberg, C. D. Is the use of some calcium antagonists linked to cancer? Evidence from recent observational studies. *Drugs Aging* **1998**, *13*, 99–108.
(66) Kritchevsky, S. B.; Pahor, M. Calcium-channel blockers and risk of cancer. *Lancet* **1997**, *349*, 1400.
(67) Pahor, M.; Guralnik, J. M.; Ferrucci, L.; Corti, M. C.; Salive, M. E.; Cerhan, J. R.; Wallace, R. B.; Havlik, R. J. Calcium-channel blockade and incidence of cancer in aged populations. *Lancet* **1996**, *348*, 493–497.
(68) Suadicani, P.; Hein, H. O.; Gyntelberg, F. Is the use of antihypertensives and sedatives a major risk factor for colorectal cancer. *Scand. J. Gastroenterol.* **1993**, *28*, 475–481.
(69) Olsen, J. H.; Sorensen, H. T.; Friis, S.; McLaughlin, J. K.; Steffensen, F. H.; Nielsen, G. L.; Andersen, M.; Fraumeni, J. F., Jr.; Olsen, J. Cancer risk in users of calcium channel blockers. *Hypertension* **1997**, *29*, 1091–1094.
(70) Assimes, T. L.; Elstein, E.; Langleben, A.; Suissa, S. Long-term use of antihypertensive drugs and risk of cancer. *Pharmacoepidemiol. Drug Saf.* **2008**, *17*, 1039–1049.
(71) Sorensen, H. T.; Olsen, J. H.; Mellemkjaer, L.; Marie, A.; Steffensen, F. H.; McLaughlin, J. K.; Baron, J. A. Cancer risk and mortality in users of calcium channel blockers. A cohort study. *Cancer* **2000**, *89*, 165–170.
(72) Shadman, M.; Newcomb, P. A.; Hampton, J. M.; Wernli, K. J.; Trentham-Dietz, A. Non-steroidal anti-inflammatory drugs and statins in relation to colorectal cancer risk. *World J. Gastroenterol.* **2009**, *15*, 2336–2339.
(73) Etminan, M.; Coogan, P. F.; Rosenberg, L. Statins and cancer: will we ever know the answer? *Epidemiology* **2002**, *13*, 607–608.
(74) Coogan, P. F.; Smith, J.; Rosenberg, L. Statin use and risk of colorectal cancer. *J. Natl. Cancer Inst.* **2007**, *99*, 32–40.
(75) Welch, H. G. Statins and the risk of colorectal cancer. *N. Engl. J. Med* **2005**, *353*, 952–954.
(76) Poynter, J. N.; Gruber, S. B.; Higgins, P. D.; Almog, R.; Bonner, J. D.; Rennert, H. S.; Low, M.; Greenson, J. K.; Rennert, G. Statins and the risk of colorectal cancer. *N. Engl. J. Med* **2005**, *352*, 2184–2192.
(77) Vinogradova, Y.; Hippisley-Cox, J.; Coupland, C.; Logan, R. F. Risk of colorectal cancer in patients prescribed statins, nonsteroidal anti-inflammatory drugs, and cyclooxygenase-2 inhibitors: nested case-control study. *Gastroenterology* **2007**, *133*, 393–402.
(78) Chawla, A.; Karl, P. I.; Reich, R. N.; Narasimhan, G.; Michaud, G. A.; Fisher, S. E.; Schneider, B. L. Effect of olsalazine on sodium-dependent bile acid transport in rat ileum. *Dig. Dis. Sci.* **1995**, *40*, 943–948.
(79) Hedner, T. Calcium channel blockers: spectrum of side effects and drug interactions. *Acta Pharmacol. Toxicol. (Copenhagen)* **1986**, *58* (Suppl. 2), 119–130.
(80) Rolachon, A.; Bichard, P.; Kezachian, G.; Zarski, J. P. [Chronic diarrhea caused by isradipine]. *Gastroenterol. Clin. Biol.* **1993**, *17*, 310–311.

would be significant in terms of assessing ASBT potential. However, such concentrations are generally unknown. For example, drugs with high permeability in an immediate-release formulation may be completely absorbed before reaching the terminal ileum. Therefore, simple application of inhibitory K_i values cannot anticipate disease risk.

In summary, this study has indicated the value of using *in silico* and *in vitro* approaches to identify novel inhibitors of ASBT that are also FDA-approved drugs. A 3D-QSAR and Bayesian model of ASBT have been successfully developed. In the future, a broader search could be applied to include several thousand other FDA-approved drugs currently on the market or drugs approved overseas. In the absence of a crystal structure, such an increased scope may provide novel insights into the molecular interaction of inhibitors with ASBT.

Abbreviations Used

ASBT, apical sodium-dependent bile acid transporter; MDCK, Madin-Darby canine kidney; HBSS, Hanks' balanced salt solution; CCBs, calcium channel blockers; NSAIDs, nonsteroidal anti-inflammatory drugs; SLC, solute carrier family; AIC, Akaike Information Criterion; 3D-QSAR, three-dimensional quantitative structure−activity relationship; IBAM, idiopathic intestinal bile acid malabsorption syndrome.

Acknowledgment. This work was supported in part by National Institutes of Health Grant DK67530. S.E. gratefully acknowledges Dr. Matthew D. Krasowski for his assistance in creating the SCUT 2008 database supplemented with metabolites and drugs of abuse. S.E. also thanks Accelrys (San Diego, CA) for making Discovery Studio Catalyst available.

Supporting Information Available: SCUT database search results and some model performance results. This material is available free of charge via the Internet at http://pubs.acs.org.

MP900163D